

## Nonequilibrium plasmon emission drives ultrafast carrier relaxation dynamics in photoexcited graphene

J. M. Hamm,<sup>1,\*</sup> A. F. Page,<sup>1</sup> J. Bravo-Abad,<sup>2</sup> F. J. Garcia-Vidal,<sup>2,3</sup> and O. Hess<sup>1,†</sup>

<sup>1</sup>*Blackett Laboratory, Department of Physics, Imperial College London, London SW7 2AZ, United Kingdom*

<sup>2</sup>*Departamento de Física Teórica de la Materia Condensada and Condensed Matter Physics Center (IFIMAC), Universidad Autónoma de Madrid, E-28049 Madrid, Spain*

<sup>3</sup>*Donostia International Physics Center (DIPC), E-20018 Donostia/San Sebastian, Spain*

(Received 5 June 2015; revised manuscript received 15 December 2015; published 11 January 2016)

The fast decay of carrier inversion in photoexcited graphene has been attributed to optical phonon emission and Auger recombination. Plasmon emission provides another pathway that, as we show here, drives the carrier relaxation dynamics on ultrafast time scales. In studying the nonequilibrium relaxation dynamics we find that plasmon emission effectively converts inversion into hot carriers, whose energy is then extracted by optical phonon emission. This mechanism not only explains the observed femtosecond lifetime of inversion but also offers the prospect for atomically thin ultrafast plasmon emitters.

DOI: [10.1103/PhysRevB.93.041408](https://doi.org/10.1103/PhysRevB.93.041408)

Graphene owes its extraordinary electronic, optical, and plasmonic properties [1–5] to the presence of Dirac points in its band structure, in the vicinity of which electrons are described as massless Dirac fermions (MDFs). One of graphene's unique characteristics is that low-energy pair excitations can decay into plasmons [6,7], a process that is kinematically forbidden in most three-dimensional and two-dimensional (2D) materials.

When excited with a femtosecond optical pulse, a hot carrier plasma is generated, which rapidly thermalizes into a state of quasiequilibrium due to carrier-carrier scattering on 10-fs scales [8,9]. After thermalization, electrons and holes recombine via interband scattering processes, effectively depleting carrier inversion over time [10,11]. Femtosecond pump-probe experiments [12–14] and time- and angle-resolved photoemission spectroscopy [15–17] indicate the presence of two dominant recombination channels: a slow decay on a 1-ps scale due to emission of optical phonons [18–20], whose signatures can be observed by Raman spectroscopy, and a fast decay on a 100-fs scale that has been attributed to Auger recombination (AR) [14,21]. This interpretation remains subject to discussion as AR processes are suppressed when considering dynamic screening in random-phase approximation [22,23].

In this Rapid Communication we show that nonequilibrium plasmon emission (NPE) (see Fig. 1) provides an alternative pathway for carrier relaxation that drives the decay of inversion on a 100-fs scale. It was recently established that plasmon emission in inverted graphene is ultrafast, with rates that exceed those of optical phonon emission by at least one order of magnitude [24,25]. However, in assuming predefined carrier and plasmon distributions, these works did not account for the dynamic evolution of the coupled carrier-plasmon system far from equilibrium. Thus, despite the prediction of ultrafast rates, it remains an open question how NPE impacts the relaxation dynamics, as plasmons are not only constantly emitted but also absorbed back into the electron/hole plasma. Ultimately, to assess the importance of NPE as a channel

for carrier relaxation, it is necessary to study the temporal evolution of the nonequilibrium plasmon distribution in interaction with the inverted carrier system, and together with optical phonon emission, which provides additional pathways for carrier recombination and cooling. As we will show, an interplay of channels emerges, where NPE drives the ultrafast conversion of inversion into hot carriers on 100-fs scales, while optical phonons efficiently extract heat from the MDF plasma.

As the basis for this work we introduce nonequilibrium rate equations for an inverted MDF plasma in interaction with bosonic reservoirs via emission and absorption processes. In quasiequilibrium, the state of the inverted carrier plasma is characterized by chemical potentials  $\mu^\alpha$  ( $\alpha = e, h$ ) for the electrons and holes and a common plasma temperature  $T_c$ , whose temporal changes can be expressed by those of the carrier densities  $N^\alpha = N(\mu^\alpha, T_c)$  of electron and holes and the total energy density  $U = U^e + U^h$  of the plasma [where  $U^\alpha = U(\mu^\alpha, T_c)$ ] (see [27], Sec. I). We split the time derivatives into optical excitation (pump) and relaxation terms,

$$\dot{N}^\alpha = \dot{N}|_{\text{pump}} - \dot{N}|_{\text{rel}} \quad \text{and} \quad \dot{U} = \dot{U}|_{\text{pump}} - \dot{U}|_{\text{rel}}, \quad (1)$$

where  $\dot{N}^e = \dot{N}^h$  as particles and holes are created (and annihilated) pairwise. For quasimonochromatic excitation with frequency  $\hbar\omega$  and intensity  $I_\omega(t)$  the pump terms are given by  $\dot{N}|_{\text{pump}} = \text{Re}[\sigma_{\text{inter}}(\omega)]|E_\omega(t)|^2/(2\hbar\omega)$  and  $\dot{U}|_{\text{pump}} = \text{Re}[\sigma(\omega)]|E_\omega(t)|^2/2$ . Here  $Z_0$  is the vacuum impedance,  $|E_\omega(t)|^2 = 2Z_0|t(\omega)|^2 I_\omega(t)$  the electric field square,  $t(\omega) = [1 + Z_0\sigma(\omega)/2]^{-1}$  the transmission coefficient,  $\sigma = \sigma(\omega; \mu^e, \mu^h, T_c)$  the optical conductivity, and  $\sigma_{\text{inter}}$  its interband only contribution.

Carrier relaxation, in turn, is a result of the interaction with bosonic reservoirs, such as the plasmon and optical phonon fields [26]. The microscopic mechanisms behind the dynamic relaxation of the carrier number and energy densities are intra- and interband scattering processes, as given by Boltzmann collision integrals. To account for the various bosonic reservoirs ( $\nu$ ), as well as intra- and intraband transitions ( $\lambda$ ), we write [20]

$$\dot{N}|_{\text{rel}} = \sum_\nu R_{\nu,eh}, \quad \dot{U}|_{\text{rel}} = \sum_\nu \sum_{\lambda=ee, hh, eh} S_{\nu,\lambda}. \quad (2)$$

\*j.hamm@imperial.ac.uk

†o.hess@imperial.ac.uk

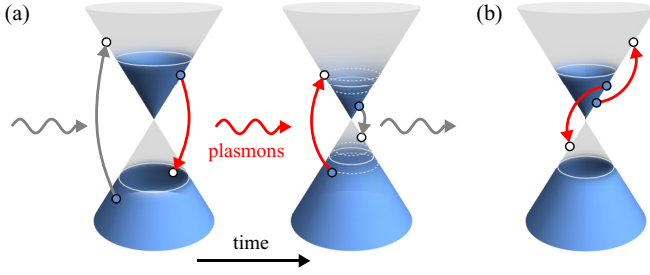


FIG. 1. Schematic of carrier recombination channels in inverted graphene. (a) Nonequilibrium plasmon emission and (b) Auger recombination both convert electron/hole pairs into hot carriers. In contrast to Auger recombination, plasmon emission is an inelastic process that is enabled by the strong coupling of electron/hole pair to 2D plasmon excitations.

The net carrier and energy relaxation rates  $R_{v,eh}$  and  $S_{v,\lambda}$  are obtained by summation over all wave-vector states  $\mathbf{q}$  of the reservoir bosons, i.e.,

$$R_{v,\lambda} = \frac{1}{A} \sum_{\mathbf{q}} r_{v,\lambda}(\mathbf{q}), \quad S_{v,\lambda} = \frac{1}{A} \sum_{\mathbf{q}} \epsilon_v(\mathbf{q}) r_{v,\lambda}(\mathbf{q}), \quad (3)$$

where

$$r_{v,\lambda}(\mathbf{q}) = \gamma_{v,\lambda}^+(\mathbf{q})[n_v(\mathbf{q}) + 1] - \gamma_{v,\lambda}^-(\mathbf{q})n_v(\mathbf{q}) \quad (4)$$

is the net spectral emission rate,  $A$  the area of the graphene sample,  $\epsilon_v(\mathbf{q}) = \hbar\omega_v(\mathbf{q})$  the energy dispersion of the boson field,  $\gamma_{v,\lambda}^+(\gamma_{v,\lambda}^-)$  the emission (absorption) rate, and  $n_v(\mathbf{q})$  the nonequilibrium distribution of the respective boson field. Within the framework of Boltzmann kinetic equations and the relaxation time approximation for collision processes, the temporal evolution of the bosonic distribution function is given by [11,20,21]

$$\dot{n}_v(\mathbf{q}) = \sum_{\lambda=ee, hh, eh} r_{v,\lambda}(\mathbf{q}) - \tau_v^{-1} [n_v(\mathbf{q}) - n_v^{(eq)}(\epsilon_v(\mathbf{q}), T_0)], \quad (5)$$

with a collision rate  $\tau_v^{-1}$ , and the equilibrium distribution  $n_v^{(eq)}(\epsilon, T_0)$  of the reservoir at ambient temperature  $T_0$ . Note that, as  $n_v(\mathbf{q})$  returns to equilibrium,  $r_{v,\lambda}(\mathbf{q})$  becomes zero according to the condition of detailed balance.

Equipped with these equations, we proceed to study the carrier relaxation dynamics for interaction with the plasmon reservoir and then under the inclusion of phonon channels. The results in this work are obtained by integrating Eqs. (2) and (5) over time. For all our simulations we consider a suspended sheet of graphene at ambient temperature that is excited by a pulse with a fluence of  $133 \mu\text{J}/\text{cm}^2$  and a photon energy of 1 eV. To enforce the same initial conditions for all simulations, we keep all relaxation channels switched off during optical excitation. Under these conditions the excitation pulse creates a thermalized inverted state with chemical potentials  $\mu^e = \mu^h \approx 0.3$  eV and a carrier temperature  $T_c \approx 2288$  K.

When the carrier system of graphene is inverted, electron/hole pair excitations and plasmons interact strongly via plasmon emission and absorption processes. The associated spectral rates can be calculated approximatively using Fermi's golden rule, with an accuracy that critically depends on

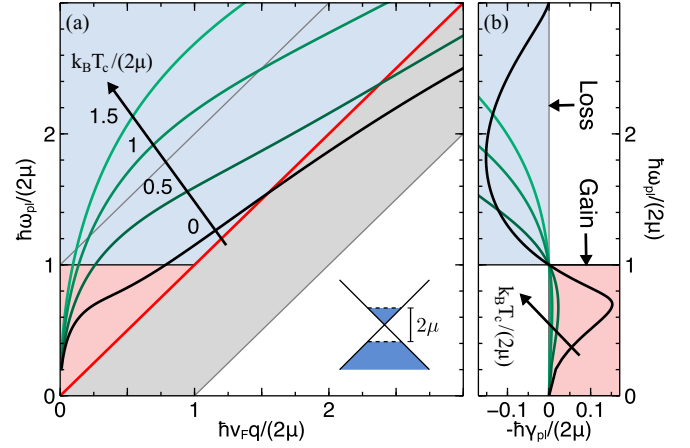


FIG. 2. (a) Plasmon frequency dispersion  $\omega_{pl}(q)$  and (b) loss spectrum  $\gamma_{pl}(\omega)$  of intrinsic graphene for varying temperature  $T_c$  scaled with chemical potential  $\mu$ . The dispersion crosses through regimes of interband gain (red area) and absorption (blue area). For  $\mu = 0.1$  eV temperatures shown range from  $T_c = 0$ –3208 K.

the exactness of the plasmon frequency dispersion  $\omega_{pl}(q)$  [25]. Therefore we trace the exact *complex-frequency* roots  $\omega(q) = \omega_{pl}(q) - i\gamma_{pl}(q)$  of the dynamic dielectric function, i.e., the solutions of

$$\epsilon_{\text{RPA}}(q, \omega) = 1 - V_q \Pi_{\mu^e, \mu^h}^{T_c}(q, \omega) = 0. \quad (6)$$

Here  $V_q = e^2/(2\epsilon_0 q)$  is the bare 2D Coulomb potential and  $\Pi_{\mu^e, \mu^h}^{T_c}(q, \omega)$  the irreducible nonequilibrium polarizability of inverted graphene at temperature  $T_c$ . Figure 2 shows frequency dispersion  $\omega_{pl}(q)$  and the loss spectrum  $\gamma_{pl}(\omega) = \gamma_{pl}[q_{pl}(\omega)]$  for temperatures  $k_B T_c / (2\mu)$  in the range of 0–1.5. Plasmons experience interband gain for  $\hbar\omega_{pl} < 2\mu$  (red area) and inter- and intraband loss for  $\hbar\omega_{pl} > 2\mu$  (blue and gray areas) at all temperatures, as evident from the change of sign of the net stimulated absorption rate  $\gamma_{pl}^{\text{stim}}(\omega) = 2\gamma_{pl}(\omega)$ . Note, for our analysis, it is sufficient to consider interband processes only, as reabsorption above the Fermi edge rapidly depletes the plasmon mode population before entering the intraband regime. The respective interband emission/absorption rates are given by

$$\gamma_{pl, eh}^{\pm}(q) \approx \frac{2\alpha_g \theta(\omega - v_F q)}{\sqrt{\left(\frac{\omega}{v_F q}\right)^2 - 1}} \left. K_{eh}^{\pm} |_{\mu^e, \mu^h}^{T_c}(q, \omega) \right|_{\omega=\omega_{pl}(q)}. \quad (7)$$

Here  $\alpha_g = \alpha_f c / v_F \approx 300/137$  is the fine-structure constant of graphene and  $K_{eh}^{\pm} |_{\mu^e, \mu^h}^{T_c}(q, \omega)$  a dimensionless measure for the phase space of the absorption and emission processes (see [27], Sec. II). In addition to these processes, one needs to consider the loss of plasmons due to collisions [28], which emerges as a result of various elastic and inelastic velocity scattering processes [29]. Values for  $\tau_{\text{coll}}$  are typically in the 50–500 fs range, depending on carrier temperature, chemical potentials, and impurity concentration. While collision loss only weakly impacts on the frequency dispersion  $\omega_{pl}(q)$  [25], it serves as a secondary decay channel as plasmons purged from the reservoir are not available for reabsorption at later times.

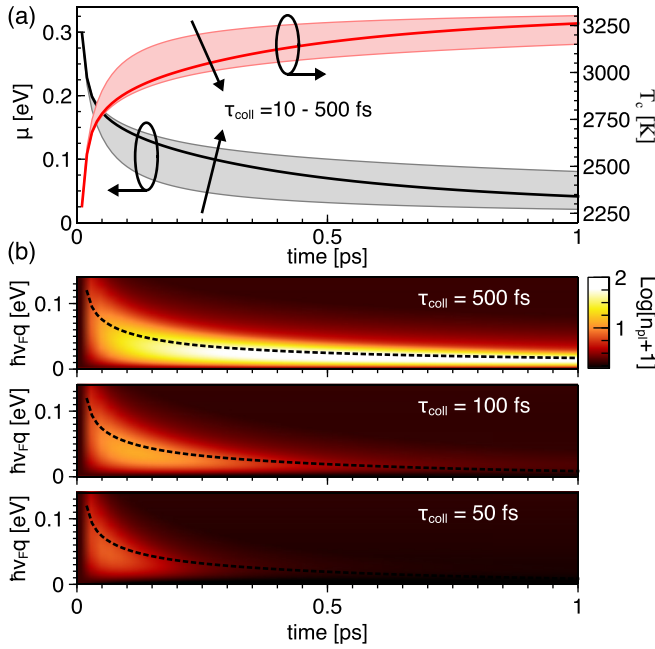


FIG. 3. Relaxation dynamics of the coupled electron/hole and plasmon system. (a) Chemical potential  $\mu$  (black) and carrier temperature  $T_c$  (red) for  $\tau_{\text{coll}} = 100$  fs (solid lines) and varying collision time (shaded area). (b) Temporal evolution of nonequilibrium plasmon distributions  $n_{\text{pl}}(q)$  and emission/absorption edge (black dashed lines).

We first study the interaction of carriers with plasmons in isolation, i.e., without inclusion of the optical phonon channels. Figure 3 shows the evolution of the chemical potential ( $\mu = \mu^e = \mu^h$ ) and the carrier temperature  $T_c$  for varying collision times, together with the temporal traces of the nonequilibrium plasmon distribution  $n_{\text{pl}}(q)$ . Within the first 100 fs after photoexcitation, a burst of plasmon emission occurs that leads to a drop of inversion (solid black line) to roughly half its initial value; at the same time, the carrier temperature (solid red line) increases by around 500 K [see Fig. 3(a)] as plasmons are emitted below the Fermi edge. Over the next 200 fs the recombination process gradually slows down. This is because reabsorption of plasmons above the Fermi edge and the decrease of the plasmon emission rate with temperature creates a *plasmon emission bottleneck*. The temporal traces of the nonequilibrium plasmon distribution  $n_{\text{pl}}(q, t)$  [Fig. 3(b)] are shown together with the threshold wave vector  $q_{\text{th}}(t)$  (black dashed line) for which the net plasmon gain is zero, i.e.,  $\gamma_{\text{pl}}(q_{\text{th}}) = 0$  (no plasmon gain/loss). Below this threshold plasmons are emitted, above they are reabsorbed. Collision loss partially removes the emission bottleneck as it purges plasmons from the reservoir and thus prevents reabsorption of plasmons into the electron/hole plasma. As a result, the recombination of carriers accelerates with increasing collision rate [gray shaded area in Fig. 3(a)].

Having analyzed the plasmon channel in isolation, we next study the interplay of NPE and optical phonon emission, which plays a pivotal role as they facilitate the recombination of electron/hole pairs [19], the cooling of hot carriers [20], as well as collision loss [30]. In inverted graphene, or at high

temperature, the inter- and intraband emission of longitudinal and transverse optical phonons are dominant channels for carrier recombination and cooling. For this work we consider all relevant optical phonon channels, the  $\Gamma\text{O}$ , the  $\text{KO}$ , and the  $\text{KA}$  phonons with energies of  $\epsilon_{\Gamma\text{O}} = 196$  meV,  $\epsilon_{\text{KO}} = 160$  meV, and  $\epsilon_{\text{KA}} = 120$  meV, respectively [31,32]. As the optical phonon modes are quasi-dispersion-free, Eq. (3) reduces to  $R_{\nu,\lambda} = \Gamma_{\nu,\lambda}^+[n_\nu + 1] - \Gamma_{\nu,\lambda}^- n_\nu$  and  $S_{\nu,\lambda} = \epsilon_\nu R_{\nu,\lambda}$ , where  $n_\nu$  is the occupation number and  $\epsilon_\nu$  the phonon energy. Closed-form expressions for the rates  $\Gamma_{\nu,\lambda}^\pm = M_{\nu,\lambda} \gamma_{\nu,\lambda}^\pm$  and the phonon density of states  $M_{\nu,\lambda}$  are given in the Supplemental Material [27], Sec. III.

To understand the fundamental difference of NPE and optical phonon emission, we first consider the carrier dynamics without NPE, i.e., under inclusion of optical phonon emission only assuming a phonon decay time of  $\tau_{\text{lat}} = 2.5$  ps [20]. Figure 4(a) depicts the temporal evolution of the chemical potential (black line) together with the carrier temperature (red line) and temperatures of the  $\Gamma\text{O}$ ,  $\text{KO}$  phonons (blue lines;  $\text{KA}$  phonons omitted for clarity). The initial dip in carrier temperature (at  $t \approx 400$  fs), accompanied by a rise of phonon temperatures and chemical potential, is predominantly due to intraband phonon emission, which continuously extracts energy from the carrier plasma. As the phonon temperature equilibrates with the plasma temperature, intraband cooling becomes increasingly inefficient. Over the next 1 ps,  $\mu$  drops from 0.3 to 0.2 eV mainly due to interband emission of optical phonons. As carrier temperature and chemical potential further decrease, both inter- and intraband emission of optical phonons slows down. Less electron/hole pairs are available at the required phonon energies and carrier cooling is bottlenecked by the slow decay of optical phonons into acoustic phonons on picosecond scales.

The relaxation dynamics changes dramatically when NPE is taken into account [see Fig. 4(b)]. The rapid drop of inversion within the first 100 fs, due to the plasmon emission burst, is followed by a gradual slowdown as plasmons are reabsorbed above the Fermi edge. The plasmon energy that flows back into the electron/hole system heats the carrier plasma and thus prevents the drop in carrier temperature that was observed in Fig. 4(a). At  $t = 1$  ps the chemical potential has fallen well below 0.1 eV, compared to a value of  $\mu \approx 0.25$  eV in Fig. 4(a), where plasmon emission was switched off. Collision loss further accelerates the decay of inversion, albeit not as strongly as in Fig. 3(a) (plasmons only), as phonons now provide an efficient cooling channel that alleviates the impact of carrier heating due to plasmon reabsorption. The combination of plasmon and optical phonon emission effectively bypasses bottlenecks observed for the isolated channels, thereby accelerating the carrier recombination and cooling dynamics.

To analyze the decay of carrier inversion due to NPE we fit  $\mu(t)$  with triexponential functions  $\mu_{\text{fit}}(t) = \mu_0 \sum_{i=1}^3 A_i \exp(-t/\tau_i)$ . The extracted (effective) decay times  $\tau_i$  and relative amplitudes  $A_i$  are shown in Figs. 4(c) and 4(d) in dependence on collision time. NPE alone induces three time scales (dashed lines): a fast rate ( $\tau_1 \approx 30$  fs) that relates to the plasmon emission into unoccupied plasmon modes with an amplitude that rises quickly for  $\tau_{\text{coll}} < \tau_1$ ; a slower rate ( $\tau_1 \approx 300$  fs) due to fast emission and reabsorption at

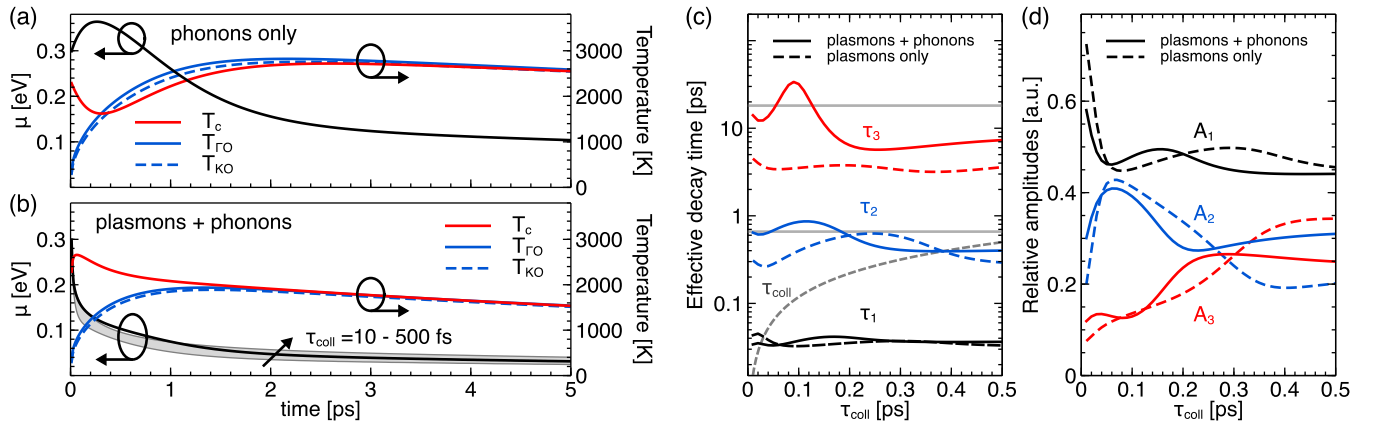


FIG. 4. Relaxation dynamics of carriers coupled to (a) phonon only and (b) plasmons and phonons where  $\tau_{\text{coll}} = 100$  fs. Shown are chemical potential  $\mu$  (black line), carrier temperature  $T_c$  (red line), and temperatures of the GO, KO phonons  $T_{\text{GO}}$  (blue solid line), and  $T_{\text{KO}}$  (blue dashed line); the gray area in (b) indicates change with collision time. (c), (d) Effective decay times  $\tau_i$  and amplitudes  $A_i$  extracted from triexponential fit to  $\mu(t)$  considering plasmons only (dashed lines) and plasmons and phonons (solid lines); gray lines indicate decay times extracted from (a) (phonons only).

the Fermi edge; and a slow rate ( $\tau_3 \approx 3$  ps) that is strongly influenced by absorption below the Fermi edge, as evident from the rise of amplitude  $A_3$  with  $\tau_{\text{coll}}$ . Activating the phonon channel in addition to NPE (solid lines) causes an interplay of channels as the NPE decay times  $\tau_2$  and  $\tau_3$  are close to the time scales that govern the decay via phonon emission [Fig. 4(c), gray lines]. This is apparent in the change of amplitudes  $A_2$  and  $A_3$ , which for  $\tau_{\text{coll}} > 200$  fs become almost constant, resulting in a decay of inversion that is almost independent of  $\tau_{\text{coll}}$  [see Fig. 4(b), gray shaded area]. Most prominently, the relaxation dynamics and extracted time scales show that inversion above  $\mu_e = \mu_h = 0.1$  eV decays on 100-fs scales due to the ultrafast decay of electron/hole pairs into plasmons.

In conclusion, we have established that plasmon emission drives the ultrafast carrier relaxation in photoexcited graphene, as 2D plasmons can couple strongly to pair excitations of the inverted carrier plasma. Our results are consistent

with the recent experimental observation of femtosecond decay of population inversion [13,15]. In contrast to Auger processes, whose experimental detection is very challenging [17], plasmon emission can be directly observed and thus provides a novel path for experimental characterization of relaxation processes. Interaction of plasmons with a (polar) substrate causes a redshift of the plasmon emission spectrum and hybridization with surface optical phonons. These effects are not expected to change the main conclusions drawn here, and will be studied in a future work.

The authors thank Fouad Ballout for discussions. This work has been funded by the Engineering and Physical Sciences Research Council (United Kingdom), the Leverhulme Trust (United Kingdom), the European Research Council (ERC-2011-AdG Proposal No. 290981) and the Spanish MINECO (Grant No. MAT2011-28581-C02-01).

- [1] A. H. Castro Neto, F. Guinea, N. M. R. Peres, K. S. Novoselov, and A. K. Geim, The electronic properties of graphene, *Rev. Mod. Phys.* **81**, 109 (2009).
- [2] F. H. L. Koppens, D. E. Chang, and F. J. García de Abajo, Graphene plasmonics: A platform for strong light-matter interactions, *Nano Lett.* **11**, 3370 (2011).
- [3] V. V. Popov, O. V. Polischuk, A. R. Davoyan, V. Ryzhii, T. Otsuji, and M. S. Shur, Plasmonic terahertz lasing in an array of graphene nanocavities, *Phys. Rev. B* **86**, 195437 (2012).
- [4] F. Bonaccorso, Z. Sun, T. Hasan, and A. C. Ferrari, Graphene photonics and optoelectronics, *Nat. Photonics* **4**, 611 (2010).
- [5] T. Stauber, Plasmonics in Dirac systems: From graphene to topological insulators, *J. Phys.: Condens. Matter* **26**, 123201 (2014).
- [6] G. F. Giuliani and J. J. Quinn, Lifetime of a quasiparticle in a two-dimensional electron gas, *Phys. Rev. B* **26**, 4421 (1982).
- [7] A. Bostwick, T. Ohta, T. Seyller, K. Horn, and E. Rotenberg, Quasiparticle dynamics in graphene, *Nat. Phys.* **3**, 36 (2007).
- [8] P. A. George, J. H. Strait, J. M. Dawlaty, S. Shivaraman, M. Chandrashekar, F. Rana, and M. G. Spencer, Ultrafast optical-pump terahertz-probe spectroscopy of the carrier relaxation and recombination Dynamics in epitaxial graphene, *Nano Lett.* **8**, 4248 (2008).
- [9] V. Ryzhii, M. Ryzhii, and T. Otsuji, Negative dynamic conductivity of graphene with optical pumping, *J. Appl. Phys.* **101**, 083114 (2007).
- [10] E. Malić, T. Winzer, E. Bobkin, and A. Knorr, Microscopic theory of absorption and ultrafast many-particle kinetics in graphene, *Phys. Rev. B* **84**, 205406 (2011).
- [11] B. Y. Sun, Y. Zhou, and M. W. Wu, Dynamics of photoexcited carriers in graphene, *Phys. Rev. B* **85**, 125413 (2012).
- [12] M. Breusing, C. Ropers, and T. Elsaesser, Ultrafast Carrier Dynamics in Graphite, *Phys. Rev. Lett.* **102**, 086809 (2009).

- [13] T. Li, L. Luo, M. Hupalo, J. Zhang, M. C. Tringides, J. Schmalian, and J. Wang, Femtosecond Population Inversion and Stimulated Emission of Dense Dirac Fermions in Graphene, *Phys. Rev. Lett.* **108**, 167401 (2012).
- [14] D. Brida, A. Tomadin, C. Manzoni, Y. J. Kim, A. Lombardo, S. Milana, R. R. Nair, K. S. Novoselov, A. C. Ferrari, G. Cerullo, and M. Polini, Ultrafast collinear scattering and carrier multiplication in graphene, *Nat. Commun.* **4**, 1987 (2013).
- [15] I. Gierz, J. C. Petersen, M. Mitran, C. Cacho, I. C. E. Turcu, E. Springate, A. Stöhr, A. Köhler, U. Starke, and A. Cavalleri, Snapshots of non-equilibrium Dirac carrier distributions in graphene, *Nat. Mater.* **12**, 1119 (2013).
- [16] J. C. Johannsen, S. Ulstrup, F. Cilento, A. Crepaldi, M. Zacchigna, C. Cacho, I. C. Edmond Turcu, E. Springate, F. Fromm, C. Roidel, T. Seyller, F. Parmigiani, M. Grioni, and P. Hofmann, Direct View of Hot Carrier Dynamics in Graphene, *Phys. Rev. Lett.* **111**, 027403 (2013).
- [17] I. Gierz, F. Calegari, S. Aeschlimann, M. Chávez Cervantes, C. Cacho, R. T. Chapman, E. Springate, S. Link, U. Starke, C. R. Ast, and A. Cavalleri, Tracking Primary Thermalization Events in Graphene with Photoemission at Extreme Time Scales, *Phys. Rev. Lett.* **115**, 086803 (2015).
- [18] S. Butscher, F. Milde, M. Hirtshulz, E. Malić, and A. Knorr, Hot electron relaxation and phonon dynamics in graphene, *Appl. Phys. Lett.* **91**, 203103 (2007).
- [19] F. Rana, P. A. George, J. H. Strait, J. M. Dawlaty, S. Shivaraman, M. Chandrashekar, and M. G. Spencer, Carrier recombination and generation rates for intravalley and intervalley phonon scattering in graphene, *Phys. Rev. B* **79**, 115447 (2009).
- [20] H. Wang, J. H. Strait, P. A. George, S. Shivaraman, V. B. Shields, M. Chandrashekar, J. Hwang, F. Rana, M. G. Spencer, C. S. Ruiz-Vargas, and J. Park, Ultrafast relaxation dynamics of hot optical phonons in graphene, *Appl. Phys. Lett.* **96**, 081917 (2010).
- [21] M. Breusing, S. Kuehn, T. Winzer, E. Malić, F. Milde, N. Severin, J. P. Rabe, C. Ropers, A. Knorr, and T. Elsaesser, Ultrafast nonequilibrium carrier dynamics in a single graphene layer, *Phys. Rev. B* **83**, 153410 (2011).
- [22] A. Tomadin, D. Brida, G. Cerullo, A. C. Ferrari, and M. Polini, Nonequilibrium dynamics of photoexcited electrons in graphene: Collinear scattering, Auger processes, and the impact of screening, *Phys. Rev. B* **88**, 035430 (2013).
- [23] K. J. Tielrooij, J. C. W. Song, S. A. Jensen, A. Centeno, A. Pesquera, A. Zurutuza Elorza, M. Bonn, L. S. Levitov, and F. H. L. Koppens, Photoexcitation cascade and multiple hot-carrier generation in graphene, *Nat. Phys.* **9**, 248 (2013).
- [24] F. Rana, J. H. Strait, H. Wang, and C. Manolatu, Ultrafast carrier recombination and generation rates for plasmon emission and absorption in graphene, *Phys. Rev. B* **84**, 045437 (2011).
- [25] A. F. Page, F. Ballout, O. Hess, and J. M. Hamm, Nonequilibrium plasmons with gain in graphene, *Phys. Rev. B* **91**, 075404 (2015).
- [26] D. Pines and J. R. Schrieffer, Approach to equilibrium of electrons, plasmons, and phonons in quantum and classical Pplasmas, *Phys. Rev.* **125**, 804 (1962).
- [27] See Supplemental Material at <http://link.aps.org/supplemental/10.1103/PhysRevB.93.041408> for thermodynamic relations and derivation of plasmon and phonon rates .
- [28] T. Low and P. Avouris, Graphene plasmonics for terahertz to mid-infrared applications, *ACS Nano* **8**, 1086 (2014).
- [29] I.-T. Lin and J.-M. Liu, Terahertz frequency-dependent carrier scattering rate and mobility of monolayer and AA-stacked multilayer graphene, *Sel. Top. Quantum Electron. IEEE J.* **20**, 122 (2014).
- [30] S. Das Sarma, S. Adam, E. H. Hwang, and E. Rossi, Electronic transport in two-dimensional graphene, *Rev. Mod. Phys.* **83**, 407 (2011).
- [31] K. M. Borysenko, J. T. Mullen, E. A. Barry, S. Paul, Y. G. Semenov, J. M. Zavada, M. B. Nardelli, and K. W. Kim, First-principles analysis of electron-phonon interactions in graphene, *Phys. Rev. B* **81**, 121412 (2010).
- [32] T. Fang, A. Konar, H. Xing, and D. Jena, High-field transport in two-dimensional graphene, *Phys. Rev. B* **84**, 125450 (2011).